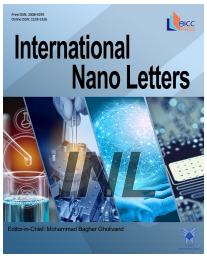

Volume 15, Issue 4, 152516 (1-6)

International Nano Letters (INL)

https://doi.org/10.57647/inl.2025.1504.16

Effect of Pulsed Laser Irradiation on Perovskite/TiO_2 Nanoparticles

Nahid Ghazyani[1,*], Vahid Kamrani Pouya[2]

[1] *Faculty of Physics, Kharazmi University, Tehran, Iran.*
[2] *Department of Materials and Metallurgical Engineering, Amirkabir University of Technology (Tehran Polytechnic), Tehran, Iran.*

[*] **Corresponding author:** Nd.ghazyani@gmail.com

Original Research

Received:
8 September 2025
Revised:
29 November 2025
Accepted:
16 December 2025
Published online:
30 December 2025

© 2025 The Author(s). Published by the OICC Press under the terms of the CC BY 4.0, Creative Commons Attribution License, which permits use, distribution and reproduction in any medium, provided the original work is properly cited.

Abstract:

Perovskite layers are key nanoscale absorbers in a wide range of optoelectronic devices, driving intense research into their deposition control, crystallization kinetics, and interfacial nanoengineering. In this work, we investigate the effects of nanosecond-pulsed Nd:YVO_4 laser irradiation (355 nm) on the structural and optical properties of perovskite layers integrated with TiO_2 nanoparticles. Nanoscale modifications induced by laser processing are systematically analyzed through optical transmission, photoluminescence (PL), surface morphology, and elemental composition measurements. The results reveal laser fluence as a decisive parameter: Low fluence deteriorates optoelectronic performance by forming a defective surface dead layer via increased nanoscale roughness, whereas higher fluence enhances optical transmittance through controlled nanoscale ablation and film thinning. Moreover, the incorporation of a mesoporous TiO_2 nanoparticle scaffold plays a critical role in maintaining bandgap stability during laser exposure, underscoring its protective function against localized thermal decomposition. These findings demonstrate that laser-matter interactions at the nanoscale can be precisely tuned to engineer perovskite layers for targeted optoelectronic device applications.

Keywords: Perovskite; TiO_2 nanoparticles; Photoluminescence; Laser process

Cite this article: Ghazyani, N., Kamrani Pouya, V. Effect of Pulsed Laser Irradiation on Perovskite/TiO_2 Nanoparticles. *Int. Nano Lett.* **15**(4), 152516 (2025).

1. Introduction

Halide perovskites (ABX_3) have revolutionized optoelectronics by bridging the gap between the low-cost processability of organics and the high performance of inorganic semiconductors. In just over a decade, their power conversion efficiency (PCE) has surged from 3.8% to over 26%, rivaling developed silicon technologies [1, 2]. This rapid progress is underpinned by the material's tunable crystal chemistry, where compositional engineering such as the shift from methylammonium (MA) to more stable formamidinium (FA) and mixed-cation (Cs/FA/Rb) formulations has significantly enhanced film quality and phase stability [3, 4]. Furthermore, adjusting the halide composition allows for precise bandgap tuning, though this is often accompanied by challenges like phase segregation under illumination [5]. The superior optoelectronic properties of perovskites, including high absorption coefficients, long carrier diffusion lengths, and low exciton binding energies, make them ideal for diverse applications beyond photovoltaics, such as light-emitting diodes (PeLEDs) and high-sensitivity X-ray detectors [6–8]. Despite their relative "defect tolerance," the performance of polycrystalline films is frequently limited by surface and grain boundary defects. These undercoordinated sites act as non-radiative recombination centers, limiting open-circuit voltage and serving as entry points for environmental degradation [9–12]. Consequently, surface engineering has become essential for passivating these defects and blocking moisture ingress.

While chemical passivation methods (e.g., 2D/3D heterostructures) are effective, they risk solvent damage or introduce unwanted residues [10]. Physical methods, particularly laser-based processing, have emerged as a powerful alternative. Laser treatment offers localized, non-contact, and solvent-free modification, enabling high surface temperatures without overheating the underlying substrate [13]. Depending on the fluence, the interaction can be photothermal-

melting the surface to enlarge grains or photochemical. In the low-fluence regime, lasers can heal defects, though excessive roughening can create a dead layer that quenches photoluminescence [11]. At higher fluences, controlled ablation thins the film and removes degraded surface layers, thereby minimizing self-absorption and restoring optical performance [14]. This precision also allows for scribing required for module interconnection [15]. Ultimately, laser engineering provides a scalable route to decouple the thermal requirements of the perovskite from the limitations of the device stack, offering a promising pathway for commercial optimization.

2. Experimental details

Film preparation: In optoelectronic devices, the perovskite layer primarily functions as the light absorber and is typically deposited onto a transparent mesoporous semiconductor, such as titanium dioxide (TiO_2). The fabrication process began with sequential cleaning of Glass/FTO substrates using a diluted detergent, deionized water, and isopropanol for 15 minutes each in an ultrasonic bath. Following this, the substrates were dried and subjected to UV-Ozone treatment for 20 minutes. A compact TiO_2 layer was then applied via spin-coating a solution of titanium acetylacetonate in anhydrous ethanol, followed by sintering at 500 °C for 30 minutes. To create the mesoporous layer, a paste of TiO_2 nanoparticles (PST-20T, IRASOL) was diluted in anhydrous ethanol and spin-coated at 4000 rpm for 30 seconds. This layer was then heated at 100 °C for 10 minutes and sintered at 500 °C for 30 minutes. Finally, the triple-cation perovskite ($Cs_{0.05}FA_{0.81}MA_{0.14}PbI_{2.55}Br_{0.45}$) was deposited by applying 30 µL of a 1.45 M precursor solution (in DMF:DMSO) using a two-step spin program: Accelerating to 1000 rpm for 10 seconds, followed by 6000 rpm for 30 seconds. The samples were subsequently vacuumed and annealed at 100 °C for 40 minutes.
Laser processing of films: Laser treatment on perovskite films was carried out using an Nd:YVO_4 nanosecond UV (355 nm, Eagle) laser. The laser beam was defocused at a distance of 3 cm. The desired conditions for laser application are listed in Table 1.

Characterization

The optical properties of the films were investigated using a Perkin–Elmer UV–Vis–NIR spectrometer to acquire transmission spectra. To evaluate the surface morphology and elemental composition, scanning electron microscopy (SEM) images and energy-dispersive X-ray spectroscopy (EDX) data were collected with a TESCAN field-emission SEM instrument. Additionally, photoluminescence (PL) measurements were performed using an Avantes TEC-2048 spectrometer, exciting the samples with a 405 nm diode laser.

3. Results and discussions

Optical transmission properties

The optical transmission spectra of the perovskite thin films subjected to various laser fluences are presented in figure 1. The spectra were recorded in the wavelength range of $400 - 1100$ nm to evaluate the impact of laser energy on the optical properties of the material.
Spectral features and interference all samples exhibit a characteristic absorption edge in the visible region (below ~ 700 nm), corresponding to the fundamental bandgap absorption of the perovskite material [5]. Notably, in the near-infrared region (above 700 nm), where the material becomes transparent, distinct sinusoidal oscillations (interference fringes) are observed. The presence of these Fabry-Pérot interference fringes indicates that the films possess a smooth surface and uniform thickness, allowing for the constructive and destructive interference of light reflected between the air-film and film-substrate interfaces [16]. The periodicity and amplitude of these fringes provide qualitative information regarding the film thickness and surface roughness, which vary significantly with laser treatment.
The transmittance spectra reveal a complex dependence on laser fluence, particularly in the transparent region (> 700 nm). The evolution of transmittance can be categorized into three distinct regimes based on the applied energy density:

- Low Fluence Regime (50 and 100 mJ/cm^2): Surprisingly, irradiation at lower fluences results in a decrease in transmittance compared to the reference sample (No laser). At 50 mJ/cm^2, the transmission is the lowest among all measured samples. This reduction in transmittance at low energies suggests that the laser interaction is dominated by surface roughening or the generation of defects rather than effective material removal [17]. The energy deposited is likely sufficient to induce partial decomposition or evaporation of the organic components (such as methylammonium) without completely removing the inorganic framework. This process leads to a porous or roughened surface morphology and the creation of light-scattering centers.

Table 1. Applied laser power parameters.

Pulse repetition rate (kHz)	Q pulse width (µs)	Beam width (µm)	Scan speed (mm/s)	Pulse energy (mJ/cm^2)
80	8	56	4500	50
40	20	122	5000	100
40	18	150	6000	150
50	9	337	17000	250
40	14	308	13000	300

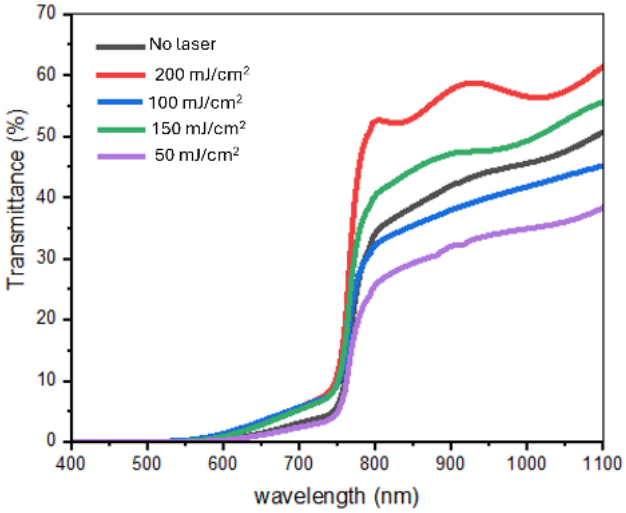

Figure 1. UV-Vis spectrum of FTO/c-TiO_2-nanoparticles TiO_2/PSK/ under different laser powers.

Consequently, increased optical scattering losses outweigh any potential benefits from thinning, resulting in lower overall transmission.

- Intermediate Fluence (150 mJ/cm^2): At a fluence of 150 mJ/cm^2, a distinct transition is observed where the transmittance exceeds that of the reference sample across the transparent region. At this energy threshold, the mechanism shifts from surface modification to material ablation. The laser energy is now sufficient to overcome the binding energy of the material, causing the effective evaporation of the perovskite layer. The reduction in film thickness becomes the dominant factor, leading to a net increase in light transmission despite the concurrent increase in surface roughness.

- High Fluence (200 mJ/cm^2): The highest transmittance is recorded at 200 mJ/cm^2. The curve is significantly elevated compared to all other samples, particularly in the $700-1100$ nm range. This behavior confirms the dominance of the ablation mechanism. The high laser energy density causes substantial thinning of the perovskite layer. According to the Beer-Lambert law, as the optical path length (thickness) decreases, transmittance increases [14]. A critical observation is that there is no significant shift in the absorption edge position across all samples. Regardless of the laser fluence, the onset of absorption remains constant in the wavelength range below 700 nm. This indicates that while the laser treatment alters the physical thickness and surface morphology (affecting scattering and magnitude of transmission), it does not significantly modify the fundamental bandgap energy or the chemical composition of the remaining perovskite scaffold.

Analysis of non-scaffolded films figure 2 presents the optical transmission spectra of perovskite layers deposited directly on glass/compact TiO_2 (without a mesoporous scaffold), subjected to varying degrees of laser treatment. To quantify the physical thickness reduction induced by the laser, the film thickness (d) was calculated geometrically using the positions of the interference fringes in the transmission spectra. The following relation was utilized for adjacent peaks at wavelengths where n is the refractive index of the perovskite. λ_1 and λ_2

$$\frac{1}{\lambda_1} - \frac{1}{\lambda_2} = \frac{1}{2nd}$$

Thickness reduction via Laser Ablation The calculated thicknesses, corresponding to the interference periods observed in the spectra, show a clear trend of thinning. The curves represent films with effective thicknesses decreasing from approximately 480 nm (gray) down to 60 nm (purple). This confirms that the laser irradiation effectively ablates the perovskite material. As the thickness decreases, the envelope of the transmission spectrum rises significantly across the measured range, consistent with the reduction in optical path length and absorption volume.

Modulation of the energy gap A distinct phenomenon observed in figure 2, which contrasts with the scaffolded samples, is the noticeable shift in the absorption edge (energy gap) concurrent with the thinning process. As the film thickness is reduced (moving from the 480 nm curve to the 60 nm curve), the absorption onset shifts to shorter wavelengths (a blue shift), indicating a widening of the optical bandgap.

In the absence of a mesoporous TiO_2 scaffold, the perovskite film is a "free-standing" layer on glass. The laser energy is absorbed directly by the perovskite without being dissipated by a scaffold network. This leads to stoichiometric decomposition effect: The intense local heating can preferentially evaporate volatile organic cations (e.g., MA^+), leading to a change in chemical composition or the formation of a PbI_2-rich surface layer, which possesses a wider bandgap than pristine perovskite [18–22].

The protective role of the Mesoporous Scaffold Comparing these results with the previous transmission spectra reveals the critical function of the mesoporous TiO_2 layer. In the scaffolded samples, the TiO_2 network acts as a thermal sink and a mechanical skeleton. It stabilizes the perovskite crystals within its pores, preventing extreme thinning and protecting the material from the thermal stress that causes chemical decomposition. Consequently, while the scaf-

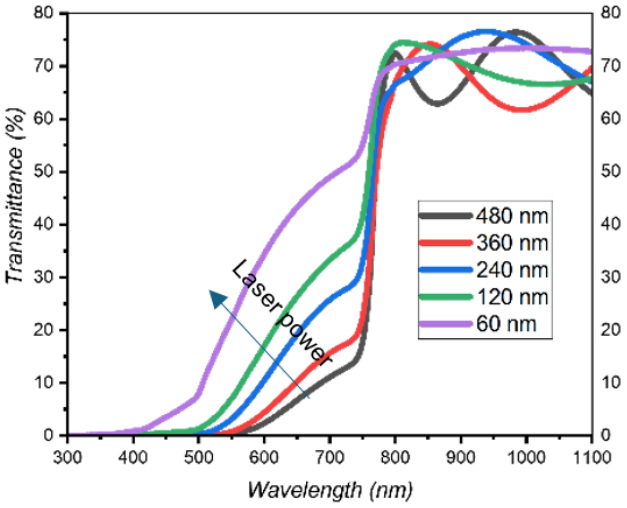

Figure 2. UV-Vis spectrum of glass/PSK films and calculated thickness.

folded samples exhibited increased transmission due to thinning, they maintained a constant energy gap [21]. In contrast, the non-scaffolded sample in figure 2 demonstrate that without this protection, laser processing not only thins the film but also degrades or fundamentally alters the electronic structure of the remaining material.

Photoluminescence (PL) analysis: The photoluminescence (PL) spectra of perovskite films (figure 3) show a distinct non-uniform dependence on laser flux. An integrated analysis, combining the intrinsic semiconductor recombination physics with the observed transmission trends (Fig. 1), reveals a complex interplay between defect dynamics and optical geometry.

- Low Power Regime (up to 100 mJ/cm^2): A significant decrease in PL intensity is observed, concomitant with a decrease in optical transmission compared to the reference sample. The decrease in PL intensity is attributed to the generation of structural defects and grain boundary disruption induced by the laser [9, 20]. These defects create non-radiative recombination centers in the bandgap that absorb photo-excited carriers and dissipate their energy as heat instead of light. This PL degradation is consistent with the transmission data, where the no laser and low-power samples show the lowest transmission. The transmission reduction in this regime is driven by light scattering (Mie scattering) due to surface roughness and lattice disorder [17], which simultaneously quench the PL. Thus, both data sets point to a degradation of the material quality and an increase in light scattering losses at low laser energies.

- High Power Regime ($150-200$ mJ/cm^2): The recovery of PL intensity is primarily controlled by the reduction of self-absorption (internal filter effect). Perovskite materials have a high absorption coefficient at their emission wavelength. In thicker layers, a large fraction of the photons generated deep in the layer are reabsorbed before they can escape [23]. As confirmed by the UV-Vis spectrum, the laser thins the layer; this reduces the optical path length and allows a larger fraction of the generated photons to escape from the surface, thereby increasing the measured external PL intensity. In addition, the erosion process probably removes the highly defective or rough surface layer formed at lower powers.

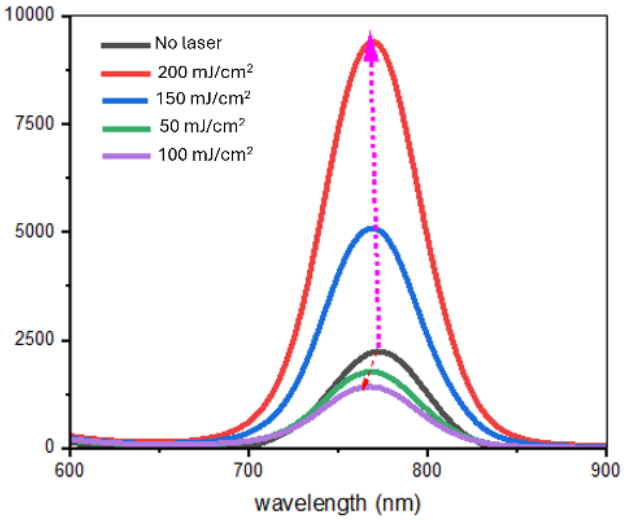

Figure 3. PL spectra of FTO/c-TiO_2-nanoparticles TiO_2/PSK/ under different laser powers.

Scanning Electron Microscopy (SEM) Analysis: The SEM images provide direct visual evidence of the physical changes occurring on the perovskite surface at various laser fluences (figure 4). The morphological evolution correlates strongly with the non-monotonic trends observed in the transmission and photoluminescence (PL) spectra.

- Reference Sample: The reference sample exhibits a uniform, continuous film composed of distinct perovskite grains. The surface appears relatively smooth with clear grain boundaries, indicative of a pristine polycrystalline structure.

- Low Fluence Regime ($50-100$ mJ/cm^2): At these fluences, the surface morphology undergoes significant changes compared to the reference. The images show a "melted" or roughened texture where the distinct grain boundaries become less defined. The surface appears porous or covered in small particles resulting from localized decomposition. These visual features confirm the formation of the dead layer [11]. The laser energy at this stage is sufficient to induce thermal stress and decomposition at the surface but not enough to remove the material. This degraded, rough layer acts as a scattering center (decrease in transmission) and introduces non-radiative recombination sites (quenching of PL).

- Intermediate Fluence (150 mJ/cm^2): At 150 mJ/cm^2, the SEM image reveals the transition from surface roughening to material removal. Distinct features such as pinholes, craters, or the beginning of film perforation become visible. This marks the threshold where laser ablation overcomes the material's cohesion. The removal of the heavily degraded top layer (the dead layer) begins here, aligning with the recovery of transmission and initial increase in PL.

- High Fluence Regime ($250-300$ mJ/cm^2): At the highest fluences, the SEM images show a dramatic reduction in surface coverage. The perovskite layer appears as isolated islands or a very thin, discontinuous network, with large areas of the underlying substrate exposed. The grain structure is destroyed or heavily modified into a resolidified surface. These images provide the visual proof of the thinning mechanism deduced from the transmission spectra. The drastic reduction in material volume explains the high transmission values and the reduction of self-absorption for PL.

Energy-Dispersive X-ray spectroscopy (EDX) analysis: As shown in figure 5, the most prominent feature in the EDX spectra is the variation in the intensity (counts) of the characteristic peaks for Lead (Pb Mβ) and Iodine (I Lα) as the

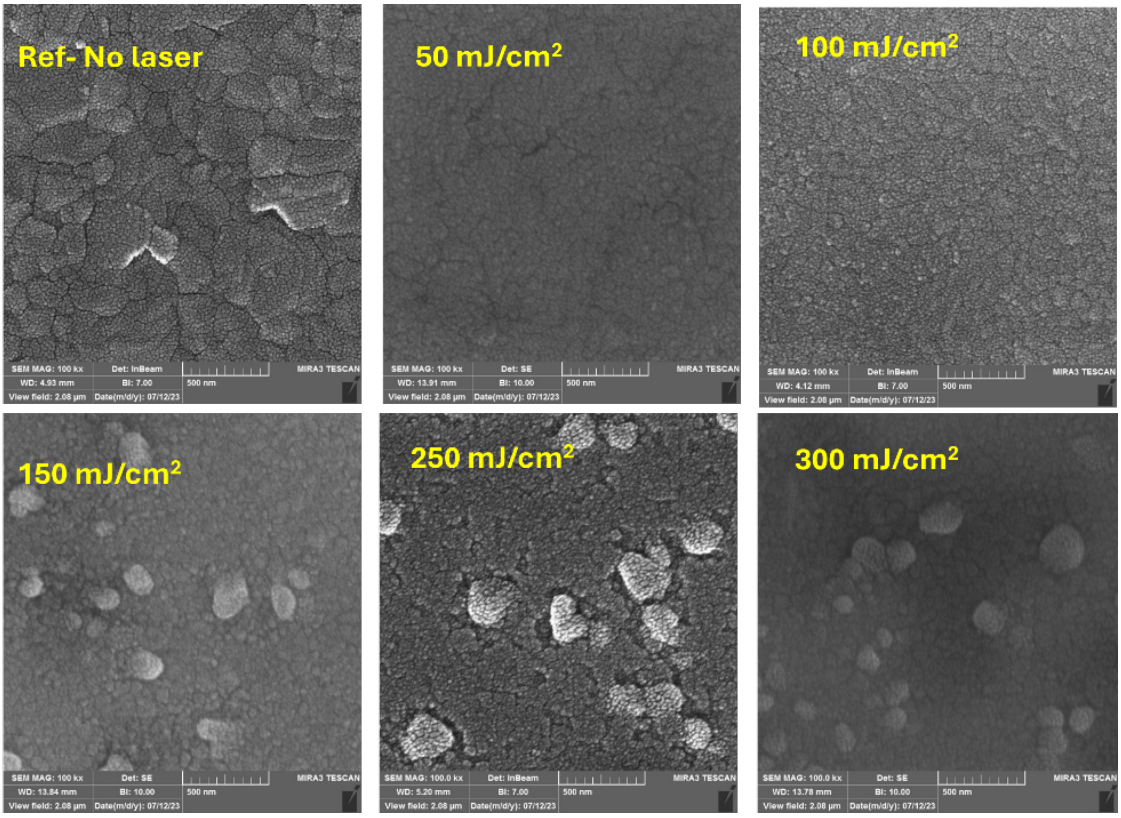

Figure 4. Top-view field emission scanning electron microscopy (FESEM) image of the glass/FTO/compact TiO_2/mesoporous nanoparticles TiO_2/PSK ($Cs_{0.05}(MA_{0.83}FA_{0.17})_{0.95}Pb(Br_{0.17}I_{0.83})_3$) under different laser powers.

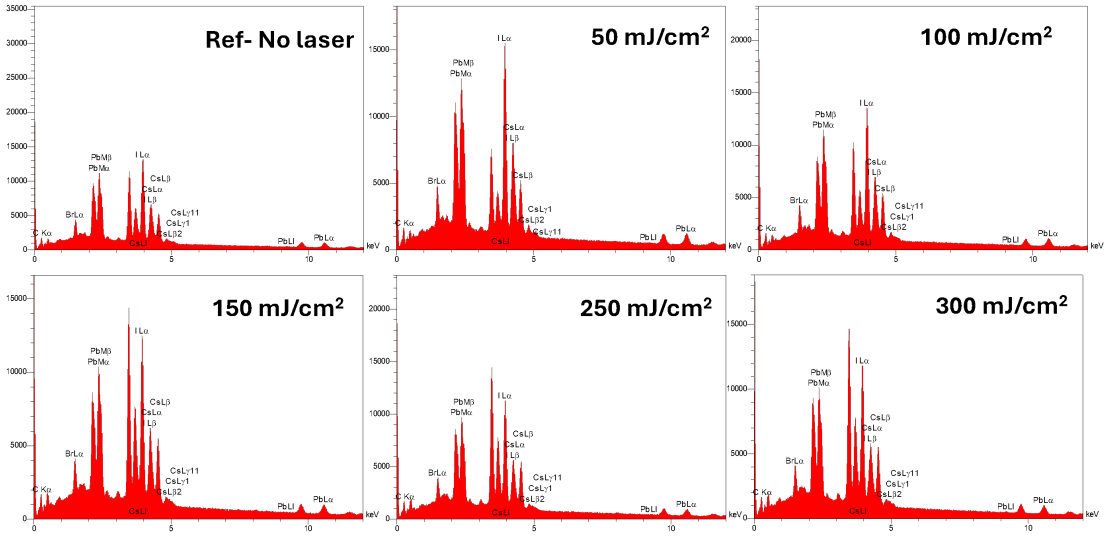

Figure 5. EDX spectrum of FTO/c-TiO_2-nanoparticles TiO_2/PSK/ under different laser powers.

laser power increases.

Physical ablation: As the laser fluence increases from No laser to 300 mJ/cm^2, the intensity of the Pb and I peaks decreases significantly. Since the X-ray signal intensity is directly proportional to the volume of material present, this reduction confirms the thinning of the perovskite layer [14]. At the highest fluences, the drastic drop in peak intensity suggests the film has become extremely thin or discontinuous.

4. Conclusion

This study demonstrates that laser fluence is a critical parameter for tuning perovskite optical properties, revealing distinct mechanisms based on power and architecture. In scaffolded samples, low fluence degrades performance through scattering and the formation of a dead layer, while high fluence enhances transmittance via ablation and thinning without altering the bandgap. Conversely, non-scaffolded films exhibit bandgap widening due to decomposition, highlighting the scaffold's essential role in

maintaining structural stability. The PL data corroborates this transition, showing initial quenching from chemical defects followed by recovery as ablation removes the degraded surface and minimizes self-absorption. Finally, SEM and EDX analyses visually and chemically validate these findings, distinguishing between chemical degradation at low powers (strong Pb/I peak) and effective physical ablation (weak) at high powers. These results indicate that laser-based optimization is a viable tool for controlling thickness and surface properties in perovskite devices.

Authors Contribution
All authors contributed equally to the conception, design, execution, and writing of this work. All authors read and approved the final manuscript.

Availability of data and materials
The data that support the findings of this study are available from the corresponding author, upon reasonable request.

Conflict of interests
The authors declare that they have no known competing financial interests or personal relationships that could have appeared to influence the work reported in this paper.

References

[1] A. Kojima, K. Teshima, Y. Shirai, and T. Miyasaka. Organometal halide perovskites as visible-light sensitizers for photovoltaic cells. *Journal of the American Chemical Society*, 131(17):6050–6051, (2009).

[2] Best Research-Cell Efficiency Chart. National Renewable Energy Laboratory (NREL). (2024). URL https://www.nrel.gov/pv/cell-efficiency.html.

[3] M. Saliba, T. Matsui, K. Domanski, J. Y. Seo, A. Ummadisingu, S. M. Zakeeruddin, and M. Grätzel. Incorporation of rubidium cations into perovskite solar cells improves photovoltaic performance. *Science*, 354(6309):206–209, (2016).

[4] D. P. McMeekin, G. Sadoughi, W. Rehman, G. E. Eperon, M. Saliba, M. T. Hörantner, and H. J. Snaith. A mixed-cation lead mixed-halide perovskite absorber for tandem solar cells. *Science*, 351(6269): 151–155, (2016).

[5] E. T. Hoke, D. J. Slotcavage, E. R. Dohner, A. R. Bowring, H. I. Karunadasa, and M. D. McGehee. Reversible photo-induced trap formation in mixed-halide hybrid perovskites for photovoltaics. . *Chemical Science*, 6(1):613–617, (2015).

[6] S. D. Stranks et al. Electron-hole diffusion lengths exceeding 1 micrometer in an organometal trihalide perovskite absorber. *Science*, 342(6156):341–344, (2013).

[7] Y.-H. Kim et al. Multicolored organic/inorganic hybrid perovskite light-emitting diodes. *Advanced Materials*, 27(7):1248–1254, (2015).

[8] Y. C. Kim, K. H. Kim, D. Y. Son, D. N. Jeong, J. Y. Seo, and N. G. Choi, Y. S. nad Park. Printable organometallic perovskite enables large-area, low-dose X-ray imaging. *Nature*, 550(7674): 87–91, (2017).

[9] W. J. Yin, T. Shi, and Y. Yan. Unusual defect physics in $CH_3NH_3PbI_3$ perovskite solar cell absorber. . *Applied Physics Letters*, 104(6), (2014).

[10] G. Grancini, C. Roldán-Carmona, I. Zimmermann, E. Mosconi, X. Lee, D. Martineau, and M. K. Nazeeruddin. One-Year stable perovskite solar cells by 2D/3D interface engineering. *Nature Communications*, 8(1):15684, (2017).

[11] L. C. Chen, C. C. Chen, J. C. Chen, and C. G Wu. Annealing effects on high-performance $CH_3NH_3PbI_3$ perovskite solar cells prepared by solution-process. *Solar Energy*, 122:1047–1051, (2015).

[12] M. B. Johnston and L. M. Herz. Hybrid perovskites for photovoltaics: Charge-carrier recombination, diffusion, and radiative efficiencies. *Accounts of Chemical Research*, 49(1):146–154, (2016).

[13] J. W. Lee and S. M. Kang. Patterning of metal halide perovskite thin films and functional layers for optoelectronic applications. *Nano-Micro Letters*, 15(1):184, (2023).

[14] F. Behrouznejad, Y. Zhan, and N. Taghavinia. UV Laser Scribing for Perovskite Solar Modules Fabrication, Pros, and Cons. *IEEE Journal of Photovoltaics*, 14(4):592–601, (2024).

[15] K. G. Brooks and M. K. Nazeeruddin. Laser processing methods for perovskite solar cells and modules. *Advanced Energy Materials*, 11 (29):2101149, (2021).

[16] D. P. McMeekin, Z. Wang, W. Rehman, F. Pulvirenti, J. B. Patel, N. K. Noel, and H. J. Snaith. Crystallization kinetics and morphology control of formamidinium–cesium mixed-cation lead mixed-halide perovskite via tunability of the colloidal precursor solution. *Advanced Materials*, 29(29):1607039, (2017).

[17] W. Tress, N. Marinova, T. Moehl, S. M. Zakeeruddin, M. K. Nazeeruddin, and M. Grätzel. Understanding the rate-dependent J–V hysteresis, slow time component, and aging in $CH_3NH_3PbI_3$ perovskite solar cells: The role of a compensated electric field. *Energy & Environmental Science*, 8(3):995–1004, (2015).

[18] T. M. Brenner, D. A. Egger, L. Kronik, G. Hodes, and D. Cahen. Hybrid organic-inorganic perovskites: Low-cost semiconductors with intriguing charge-transport properties. *Nature Reviews Materials*, 1 (1):1–16, (2016).

[19] Q. Zhang, M. Tai, Y. Zhou, Y. Zhou, Y. Wei, C. Tan, and H. Lin. Enhanced photocatalytic property of γ-CsPbI3 perovskite nanocrystals with WS2. *ACS Sustainable Chemistry & Engineering*, 8(2): 1219–1229, (2019).

[20] J. Ye, M. M. Byranvand, C. O. Martínez, R. L. Hoye, M. Saliba, and L. Polavarapu. Defect passivation in lead-halide perovskite nanocrystals and thin films: Toward efficient LEDs and solar cells. *Angewandte Chemie*, 133(40):21804–21828, (2021).

[21] T. Leijtens, G. E. Eperon, N. K. Noel, S. N. Habisreutinger, A. Petrozza, and H. J. Snaith. Stability of metal halide perovskite solar cells. *Advanced Energy Materials*, 5(20):1500963, (2015).

[22] G. W. Adhyaksa, L. W. Veldhuizen, Y. Kuang, S. Brittman, R. E. Schropp, and E. C. Garnett. Carrier diffusion lengths in hybrid perovskites: processing, composition, aging, and surface passivation effects. *Chemistry of Materials*, 28(15):5259–5263, (2016).

[23] S. De Wolf, J. Holovsky, S. J. Moon, P. Löper, B. Niesen, M. Ledinsky, and C. Ballif. Organometallic halide perovskites: Sharp optical absorption edge and its relation to photovoltaic performance. *The Journal of Physical Chemistry Letters*, 5(6):1035–1039, (2014).